



## Water-Injection Displacement Compatibility and Economic Performance in Fracture–Matrix Cores



Haifeng Lv<sup>1</sup>, Zhaobo Gong<sup>2</sup>, Lili Lin<sup>2</sup>, Chongjun Xu<sup>3</sup>, Zhong Yan<sup>2</sup>, Hangyun Wang<sup>4\*</sup>

<sup>1</sup> Development Division, Petro China Xinjiang Oilfield Company, 834000 Karamay, China

<sup>2</sup> Branch Supervision Center of Xinjiang Oilfield Co., Ltd., CNPC, 834000 Karamay, China

<sup>3</sup> Research Institute of Exploration and Development, Petro China Xinjiang Oilfield Company, 834000 Karamay, China

<sup>4</sup> School of Resources and Safety Engineering, University of Science and Technology-Beijing, 100083 Beijing, China

\* Correspondence: Hangyun Wang (why19837256790@163.com)

Received: 10-15-2024

Revised: 11-29-2024

Accepted: 02-15-2025

**Citation:** H. F. Lv, Z. B. Gong, L. L. Lin, C. J. Xu, Z. Yan, and H. Y. Wang, “Water-injection displacement compatibility and economic performance in fracture–matrix cores,” *Acadlore Trans. Geosci.*, vol. 4, no. 1, pp. 1–12, 2025. <https://doi.org/10.56578/atg040101>.



© 2025 by the author(s). Licensee Acadlore Publishing Services Limited, Hong Kong. This article can be downloaded for free, and reused and quoted with a citation of the original published version, under the CC BY 4.0 license.

**Abstract:** The No. 8 Block of Xinjiang represents a typical ultra-low-permeability fractured oilfield in which conventional water-quality evaluation techniques fail to reproduce the water-quality evolution and associated reservoir responses that occur within fractured reservoirs. To address this limitation, a graded water-quality evaluation method and an associated apparatus tailored for water injection in ultra-low-permeability fractured reservoirs were independently developed. Using this method and apparatus, fracture-matrix core water-injection displacement experiments were conducted to quantify water-reservoir compatibility and to characterize permeability evolution in fracturematrix cores during displacement. An economic evaluation of fracture-matrix core water-injection schemes was subsequently performed. The results indicate that, for fracture-matrix cores with a permeability of 8 mD, suspended particles with a median diameter  $\leq 1.5 \mu\text{m}$  and a concentration  $\leq 8 \text{ mg/L}$  cause a total permeability impairment of  $< 20\%$ , demonstrating favorable compatibility and unobstructed migration, with particle retention concentrated primarily within fracture zones. For fractures with a permeability of 20 mD, suspended particles with a median diameter  $\leq 3 \mu\text{m}$  and a concentration  $\leq 6 \text{ mg/L}$  similarly result in permeability impairment  $< 20\%$ , indicating good compatibility and successful passage. By integrating reservoir-permeability variations and historical water-injection data, an economic assessment model that accounts for reservoir evolution, oil prices, and injected-water quality was established. The model enables the identification of water-quality standards that both ensure effective reservoir development and maintain economic viability.

**Keywords:** Fracture–matrix; Injection-water quality; Reservoir physical properties; Economic performance

### 1 Introduction

As global development of conventional oil and gas resources has intensified and energy demand continues to rise, low-permeability and ultra-low-permeability reservoirs have emerged as key replacement domains for reserve growth and production enhancement [1, 2]. These reservoirs are characterized by complex pore architectures, narrow throats, and high flow resistance, rendering water injection an essential method for maintaining reservoir pressure and improving Enhanced Oil Recovery (EOR) [3, 4]. However, the effectiveness of water-injection development is strongly governed by the quality of the injected water. Suspended solid particles, microorganisms, scaling ions, dispersed oil droplets, dissolved oxygen, and other impurities present in low-quality injection water readily induce pore-throat and fracture blockage, mineral scaling, corrosion, and biofilm formation within the reservoir. Such processes can inflict substantial reservoir damage, markedly reduce water-injection efficiency, and ultimately lower the attainable recovery factor [5–7]. Therefore, precise and scientifically grounded evaluation and control of injection-water quality constitute one of the central challenges in achieving efficient and economically viable development of low-permeability and ultra-low-permeability reservoirs.

Building upon prior research, the transport and blockage of particles within porous media are generally governed by the fundamental mechanisms of deep-bed filtration, including straining, bridging, and deposition, which

macroscopically manifest as a progressive decline in permeability with increasing injected volume. Numerous experimental and numerical studies have shown that the ratio between particle diameter and pore-throat size is the key determinant controlling whether sieve filtration, bridging blockage, or internal filter-cake formation occurs [8–10]. Pore-network modeling has further demonstrated that the transition from “straining” to “bridging” and ultimately to “complete blockage” can be rigorously constrained by probabilistic functions of the particle–pore-throat size ratio [11]. At the pore scale, this process can be described using attachment–resuspension kinetic formulations, while Computational Fluid Dynamics – Discrete Element Method (CFD–DEM) coupled simulations enable the direct tracking of particle–fluid–pore–wall interactions, thereby successfully reproducing microscale phenomena observed in laboratory experiments, including the onset of bridging, disturbances in pressure distribution, and flow-field diversion [12, 13]. However, most existing models are established upon regular, homogeneous, or single-type pore structures and primarily elucidate particle migration and blockage in idealized sandstones or homogeneous porous media. Systematic constraints remain lacking for fracture–matrix dual-porosity systems, particularly regarding the coupled “fracture capture–matrix protection” mechanism and the quantitative relationships linking engineering water-quality parameters—such as median particle diameter and suspended-particle concentration—to permeability impairment [8, 14]. Furthermore, previous experiments have revealed strong coupling among particle size, flow velocity, and ionic strength of the solution, which jointly regulate particle deposition efficiency and migration pathways [15]. Microfluidic visualization studies have shown that particles can undergo deformation-assisted passage, reversible or irreversible compression, or heterogeneous accumulation within microscale pore throats [16, 17], indicating that idealized models remain insufficient for capturing the true microscopic mechanisms.

Conventional water-quality evaluation methods for water injection commonly rely on single long-core displacement experiments, in which variations in pressure and permeability are used to infer water-quality effects. However, significant limitations are associated with these approaches, particularly when the complex geological conditions of fractured reservoirs are simulated. Such methods cannot accurately represent the influence of fractures on injected-water flow, resulting in restricted accuracy and interpretive reliability. The No. 8 Block of Xinjiang is a representative fractured ultra-low-permeability oilfield [18, 19], where strict control of injection-water quality serves as a critical determinant of development performance [20–24]. In fractured reservoirs, the complexity of fracture networks, their wide range of aperture sizes, and their interactions with the matrix frequently prevent traditional injection-water quality evaluation methods from accurately reproducing water-quality evolution and its impact on reservoir behavior [25]. Consequently, the development of a new evaluation methodology is essential for improving the efficiency of water-injection development and reducing associated environmental risks.

To overcome these limitations, a new evaluation method specifically designed for assessing injection-water quality in fractured reservoirs was developed in this study. This method integrates precise fracture control within cores, fracture monitoring, displacement experiments, and CT imaging to achieve comprehensive characterization of water-quality indicators. The approach enables more accurate representation of water-quality evolution in fractured reservoirs. Moreover, by incorporating reservoir-permeability evolution and historical injection performance, an economic assessment model was established that accounts for reservoir changes, oil prices, and injection-water quality. This model enables the effective identification of injection-water quality standards that ensure both technically sound reservoir development and economic viability, providing a reference for understanding reservoir-property evolution and economic performance in fracture–matrix ultra-low-permeability reservoirs such as those found in the No. 8 Block of Xinjiang.

## 2 Experimental Methods

### 2.1 Experimental Apparatus

A graded water-quality evaluation method and apparatus for injection water in fractured ultra-low-permeability reservoirs were independently developed for this study. The method and apparatus are designed for the graded assessment of injection-water quality during core-flooding processes, enabling more accurate classification and assessment of injection-water quality in ultra-low-permeability reservoirs. This approach provides theoretical support for efficient water-injection development in fractured reservoirs. The configuration of the apparatus is shown in Figure 1.

(a) Core-fracturing and displacement unit: This unit is used to prepare core samples containing fractures of varying geometries. By assembling fractured cores with matrix cores, the complex geological structure of fractured reservoirs is simulated. After fracturing, the water-injection process is reproduced, allowing the flow of injected water through fractured cores to be monitored in real time.

(b) Data acquisition and analysis unit: This unit is responsible for collecting and processing experimental data generated during core fracturing, displacement, and water-quality preparation. Data are analyzed through computer-controlled programs to derive graded injection-water quality results for fractured reservoirs.

(c) Power supply and water-quality control unit: This unit provides the power required throughout the core-fracturing and displacement processes and prepares injection water that meets the specified experimental water-

quality conditions.

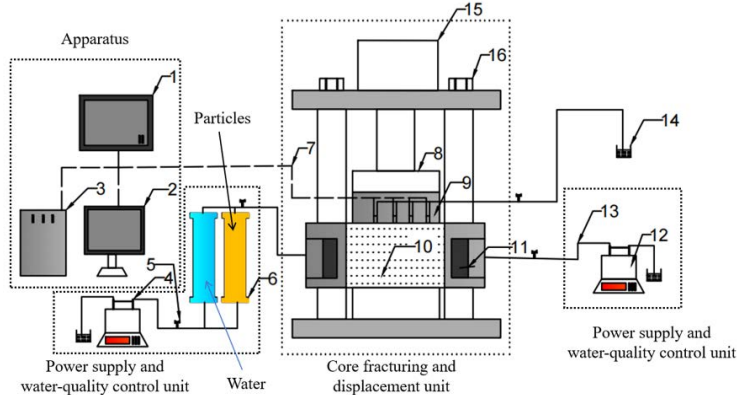


**Figure 1.** Experimental apparatus for evaluating water-injection performance in fractured ultra-low-permeability reservoirs

## 2.2 Research Procedures

The research procedures encompass the entire workflow, including core-sample preparation, fracture monitoring, displacement testing, fluid collection, data analysis, and final water-quality grading and evaluation. Each step was carefully designed to ensure comprehensive and accurate simulation of water injection in fractured reservoirs and to enable rigorous assessment of injection-water quality.

### 2.2.1 Core-sample preparation

(a) Core selection: Representative core materials, including matrix and fractured cores, were selected. The matrix cores were used to represent the rock properties of the reservoir, whereas the fractured cores were employed to reproduce the structural complexity of the fractured reservoir. Core samples were selected to ensure that porosity, permeability, and other physical parameters matched the ranges observed in field reservoirs.

(b) Fracture creation: A universal testing machine was used to induce fractures in the matrix cores, generating fractures with controlled apertures and geometries. Fracture development was regulated by adjusting pressure, loading rate, and loading-point position. During the preparation process, the fracture morphology must be monitored to ensure that fracture aperture and complexity conform to the experimental requirements. After each fracturing operation, the fracture aperture and complexity of the core were monitored in real time using acoustic probes and pressure sensors to ensure fracture stability and controllability.

(c) Core assembly: The fractured core and matrix core were subsequently assembled to form a composite core sample for testing. A high-precision fixation device was employed during assembly to ensure positional stability and prevent misalignment or damage to the cores. Following assembly, the composite core was examined using CT scanning to verify that the fracture location and morphology conform to the experimental requirements.

### 2.2.2 Fracture monitoring and dynamic control

(a) Installation of fracture-monitoring devices: Acoustic probes and pressure sensors were installed at both ends of the assembled composite core to enable real-time monitoring of fracture propagation and stability. The acoustic probes were used to detect variations in fracture aperture, with changes in acoustic-signal intensity serving as indicators of fracture opening and morphology. The probes were positioned around the circumferential bottom surface of the core, and acoustic waves were propagated along the core axis. Fracture-aperture evolution was calculated from the reflected acoustic signals received by the probes. Pressure sensors were employed to measure stress variations within the core during fracture propagation.

(b) Dynamic fracture adjustment: Based on the real-time feedback of acoustic signals and pressure variations, the loading pressure and loading rate were adjusted to ensure that the fracture aperture and complexity conformed to the experimental design specifications. If specific fracture geometries—such as intersecting fractures—were required, the loading location and direction were precisely controlled to generate the desired fracture configurations.

### 2.2.3 Displacement experiments and fluid injection

(a) Preparation for displacement experiments: The assembled fractured core was mounted in the displacement-test apparatus, which consisted of a pressure pump, a backpressure pump, and a series of fluid containers. Formation water was injected into the containers, and particles of various sizes (e.g., 1.5  $\mu\text{m}$  and 3  $\mu\text{m}$ ) were prepared to simulate particle migration under varying injection-water quality conditions.

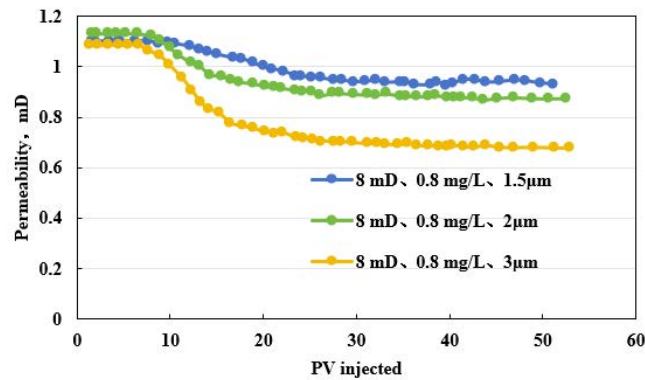
(b) Water and particle injection: During the displacement tests, formation water was injected at a constant flow rate using the pressure pump, while particles of the specified sizes (e.g.,  $1.5\text{ }\mu\text{m}$  and  $3\text{ }\mu\text{m}$ ) were simultaneously introduced. The injection of particles is intended to simulate their impact on fluid flow during water injection. Throughout the injection process, pressure variations at different positions along the core were recorded to determine whether particle-induced blockage or deep migration occurs.

(c) Fluid collection and analysis: As the fluid passed through the core specimen, multiple collection vessels were positioned to obtain effluents from different locations along the core. By adjusting the control valves, fluid samples from specific positions were collected with high spatial precision. These samples were subjected to subsequent chemical and physical analyses, including measurements of particle concentration, oil content, and microbial abundance.

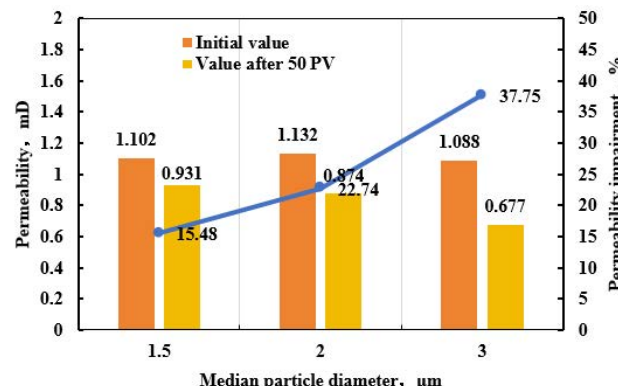
### 3 Results and Analysis

#### 3.1 Reservoir-property Evolution During Water Injection in Fracture–Matrix Cores

As shown in Figure 2, permeability progressively decreased with increasing pore-volume (PV) injection, and the magnitude of permeability reduction was strongly dependent on particle size. When small particles ( $1.5\text{ }\mu\text{m}$ ) were introduced, the decline in permeability occurred gradually, indicating a relatively weak plugging effect. As particle size increased ( $2\text{ }\mu\text{m}$  and  $3\text{ }\mu\text{m}$ ), the degree of permeability reduction became markedly more pronounced, demonstrating that larger particles induced stronger blockage within the pore networks. It is notable that permeability approached a stable value after approximately 30 PV of injection, suggesting that the dominant plugging interactions occurred during the early stages of injection, whereas the subsequent impact on permeability was comparatively limited. The bar chart further illustrates the substantial differences in permeability impairment associated with particle size. After 50 PV of injection, permeability decreased progressively as particle size increased, with the minimum permeability ( $0.677\text{ mD}$ ) observed under the  $3\text{ }\mu\text{m}$  particle condition. In terms of permeability-impairment rate, the  $1.5\text{ }\mu\text{m}$  particles produced an impairment of  $15.48\%$ , which increased to  $22.74\%$  for  $2\text{ }\mu\text{m}$  particles. The largest impairment,  $37.75\%$ , was induced by the  $3\text{ }\mu\text{m}$  particles, confirming that larger particles exerted significantly stronger plugging effects.



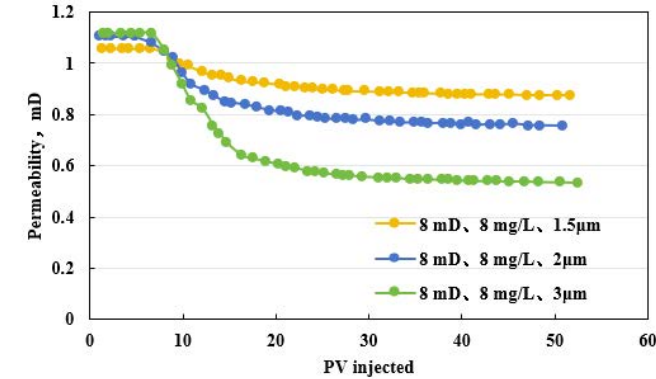
(a) Relationship between PV injection and permeability



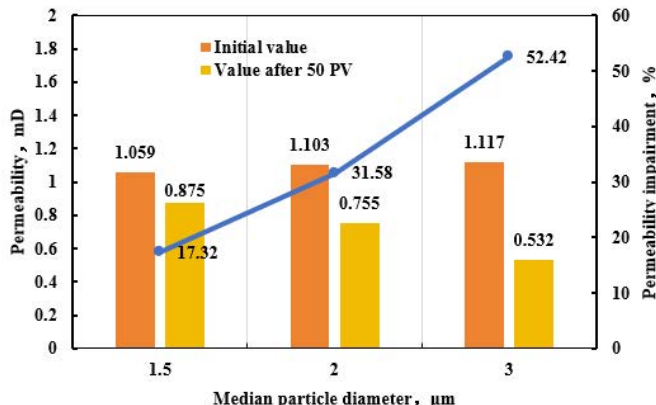
(b) Relationship between median particle diameter and permeability impairment

**Figure 2.** Impairment in a matrix–fracture system (8 mD) under different median particle diameters at  $0.8\text{ mg/L}$

The influence of particle size on core permeability was found to be highly significant. Smaller particles ( $1.5 \mu\text{m}$ ), with diameters closer to the dimensions of pore throats, were more readily transported with the flowing fluid, resulting in relatively minor plugging effects. In contrast, larger particles ( $3 \mu\text{m}$ ) were more likely to become retained or immobilized within the pore network, producing pronounced blockage and leading to substantial reductions in permeability. The variation in permeability-impairment rates further demonstrates that larger particles caused more severe damage to core permeability. This trend provides important guidance for the design of particleinjection conditions under actual reservoir environments.



(a) Relationship between PV injection and permeability



(b) Relationship between median particle diameter and permeability impairment

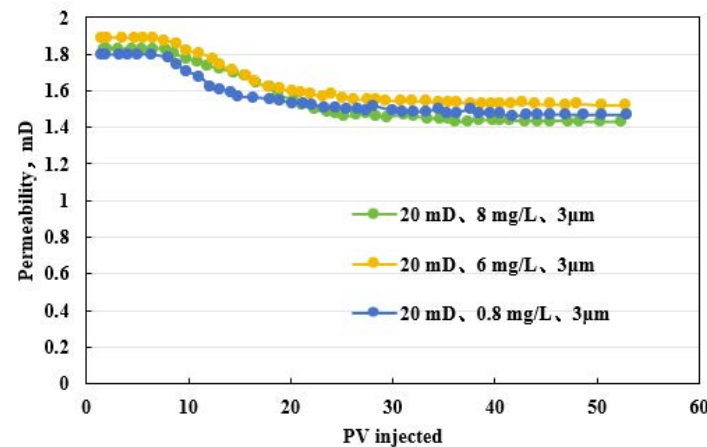
**Figure 3.** Impairment in a matrix–fracture system (8 mD) under different median particle diameters at 8 mg/L

As shown in Figure 3, a gradual decline in permeability was observed with increasing PV injection, although the magnitude of the decline varied significantly with particle size. When small particles ( $1.5 \mu\text{m}$ ) were introduced, the reduction in permeability occurred relatively slowly, indicating that the plugging effect of fine particles was weak. As particle size increased to  $2 \mu\text{m}$  and  $3 \mu\text{m}$ , the rate of permeability reduction accelerated substantially, with the  $3 \mu\text{m}$  particles producing the most pronounced decline. This trend demonstrates that larger particles were more likely to cause porethroat blockage within the core. After approximately 20 PV of injection, the permeability curves for all particle sizes gradually approached a stable state, suggesting that plugging had reached equilibrium and that subsequent changes in permeability became moderate. Following 50 PV of injection, permeability decreased markedly with increasing particle size. Under the  $3 \mu\text{m}$  particle condition, permeability declined to  $0.532 \text{ mD}$ , representing the most severe impairment. The permeability-impairment rates exhibited the same increasing trend: 17.32% for  $1.5 \mu\text{m}$  particles, 31.58% for  $2 \mu\text{m}$  particles, and 52.42% for  $3 \mu\text{m}$  particles. Fine particles ( $1.5 \mu\text{m}$ , whose diameters are closer to the pore-throat dimensions, were more easily transported with the flowing fluid and therefore induced minimal blockage. As a result, the corresponding reduction in permeability was relatively minor. In contrast, medium-sized ( $2 \mu\text{m}$ ) and large ( $3 \mu\text{m}$ ) particles were more prone to entrapment and retention within the pore network, resulting in significant plugging.

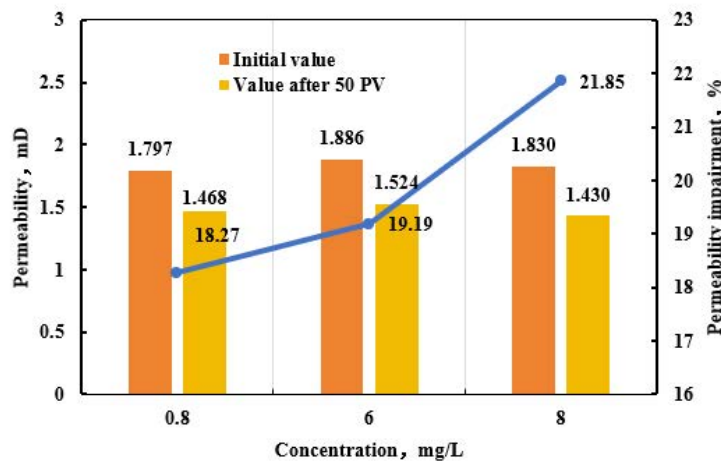
In addition, fractures played a selective filtration role by capturing upstream solid particles and effectively protecting the downstream matrix permeability. When the fracture permeability was 8 mD, suspended particles with a median diameter of  $1.5 \mu\text{m}$  at a concentration of 8 mg/L produced a total permeability-impairment rate of

less than 17.32%, indicating that the particles could pass through the fracture-matrix system smoothly. Under these conditions, particle retention occurred predominantly within the fracture segments.

As shown in Figure 4, a consistent decrease in permeability was observed with increasing PV injection, and the magnitude of this decline was positively correlated with particle concentration. At low particle concentrations (0.8 mg/L), the permeability reduction occurred gradually, indicating a relatively weak plugging effect. At higher concentrations (8 mg/L), the decline in permeability became pronounced, particularly during the early stage of injection (within the first 10 PV), when particle-induced blockage was most evident. After approximately 30 PV of injection, the permeability curves corresponding to all concentrations began to stabilize, suggesting that plugging had reached a saturation state and that additional particle accumulation exerted a diminishing incremental effect on permeability reduction. Permeability measured 1.468 mD for the 0.8 mg/L solution, whereas a more substantial reduction to 1.430 mD was observed for the 8 mg/L solution. At 0.8 mg/L, the impairment rate was 18.27%; this value increased to 19.19% at 6 mg/L and reached 21.85% at 8 mg/L. These findings indicate that higher particle concentrations intensified blockage within the pore network, resulting in more severe degradation of permeability.



(a) Relationship between PV injection and permeability



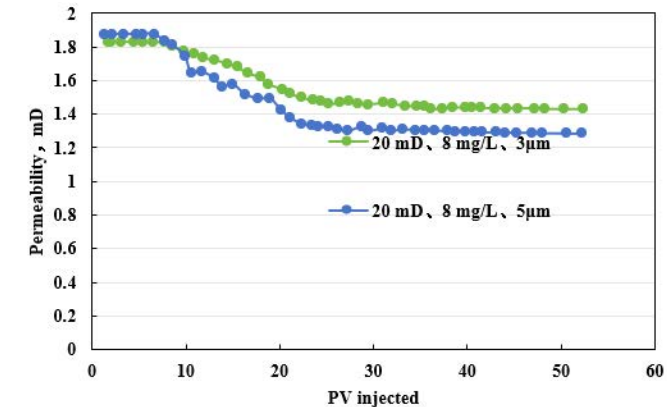
(b) Relationship between concentration and permeability impairment

**Figure 4.** Permeability impairment in a matrix–fracture system (20 mD) at different concentrations

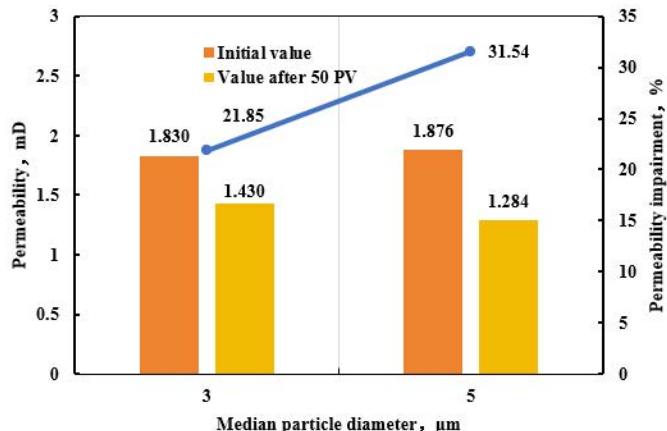
As shown in Figure 5, a progressive decrease in permeability was observed with increasing PV injection, and the rate and magnitude of this decline were strongly dependent on particle size. When the median particle diameter was 3  $\mu\text{m}$ , the reduction in permeability occurred relatively slowly, indicating a weaker plugging effect. As particle size increased to 5  $\mu\text{m}$ , the permeability decline became more rapid, particularly during the early stages of injection when particle-induced blockage was significantly intensified. After approximately 30 PV of injection, the permeability curves for both particle sizes approached a stable state, indicating that the plugging effect had reached saturation and that the incremental influence of additional particle accumulation had diminished. The bar chart shows that after 50 PV of injection, permeability decreased to 1.430 mD under the 3  $\mu\text{m}$  particle condition, whereas a more

substantial decrease to 1.284 mD occurred when 5  $\mu\text{m}$  particles were introduced. This demonstrates that larger particles produced more severe permeability impairment. Comparison of the permeability-impairment ratios showed a consistent trend in which impairment increases with particle diameter. The permeability-impairment ratio reached 21.85% for 3  $\mu\text{m}$  particles and increased to 31.54% for 5  $\mu\text{m}$  particles. These observations indicate that larger particles are more likely to induce pore blockage, resulting in more pronounced permeability losses.

Additionally, fractures exhibited a selective retention effect, trapping upstream solid particles and thereby protecting the permeability of the downstream matrix. When the fracture permeability was 20 mD, suspended particles with a median diameter of 3  $\mu\text{m}$  at a concentration of 6 mg/L resulted in an overall impairment rate of 19.19%, indicating that the suspended particles were able to pass smoothly through the fracture-matrix system.



(a) Relationship between PV injection and permeability



(b) Relationship between median particle diameter and permeability impairment

**Figure 5.** Permeability impairment in a matrix–fracture system (20 mD) under different median particle diameters

### 3.2 Economic Assessment of Reservoir Waterflooding Performance

In this study, the preliminary economic assessment was incorporated as a critical component of the water-quality decision framework. Its primary objective was to ensure that optimal economic performance could be achieved while maintaining effective reservoir development. To accomplish this, an economic assessment model that accounts for reservoir property evolution was established by integrating permeability variations with historical water-injection data.

Because of water-quality constraints, the reservoir permeability was progressively reduced during the waterflooding process. To quantitatively characterize this permeability decline, the decay rate of the unit permeability of the target reservoir—expressed as a function of the dimensionless injected volume  $Q_i$ —was obtained by fitting the experimental data under the corresponding waterquality conditions and injection history.

$$K = K_0 \alpha Q_i^{-\beta} \quad (1)$$

where,  $\alpha$  and  $\beta$  are the formation-damage coefficients ( $\times 10^{-3}$ ),  $K$  is the current reservoir permeability (mD),  $K_0$  is the reservoir permeability prior to waterflood adjustment (mD),  $Q_i$  is the dimensionless PV injected, equivalent to PV in the experiments (dimensionless), and  $\frac{dK}{dQ_i}$  is the rate of permeability variation with respect to dimensionless PV injection.

As reservoir permeability declines with increasing cumulative water injection, the change in permeability is treated as a negative value.

Based on the radial-flow productivity prediction model, the crude oil production rate under waterflooding conditions is expressed as follows:

$$q_0 = \frac{0.5428Kh(p_e - p_{wf})(1 - f_w)}{\mu_0 B_0 \ln \frac{r_e}{r_w}} = \frac{0.5428Kh(p_e - p_{wf})(1 - f_w)}{\mu_0 B_0 \ln \frac{r_e}{r_w}} \alpha Q_1^{-\beta} \quad (2)$$

where,  $q_0$  is the crude oil production rate ( $\text{m}^3/\text{d}$ ),  $h$  is the average reservoir thickness (m),  $\mu_0$  is the crude oil viscosity ( $\text{mPa} \cdot \text{s}$ ),  $p_{wf}$  is the flowing bottom-hole pressure (MPa),  $p_e$  is the supply pressure (MPa),  $r_w$  is the wellbore radius (m),  $r_e$  is the equivalent drainage radius (m), and  $f_w$  is the average water cut (%).

Building on Eq. (2), the economic benefits attributable to the water injection system after water-quality decision-making can be estimated by incorporating the cost of different water-quality options together with the crude oil price that yields economic returns. Consequently, a preliminary assessment of the economic performance of the waterflooding system can be obtained.

In the preliminary economic assessment, three primary factors are considered: (a) crude oil price, which directly governs total economic revenue; (b) water-injection cost, including water-treatment expenditure, equipment depreciation, and operational costs; (c) reservoir permeability degradation, which progressively reduces oil production as permeability declines over time. Integrating these factors yields the waterflooding economic-benefit formulation expressed in Eq. (3):

$$E = E_1 - QtE_w \quad (3)$$

where,  $E_1 = q_0 \rho_0 t E_0 = \frac{0.5428 \rho_0 K_0 h (p_e - p_{wf})(1 - f_w)}{\mu_0 B_0 \ln \frac{r_e}{r_w}} \alpha Q_1^{-\beta} t E_0$ . In addition,  $E$  is the total economic benefit (10,000CNY),  $E_1$  is the increase in revenue following water-quality decisionmaking (10,000CNY),  $E_x$  is the unit water-injection cost after water-quality adjustment (CNY/ $\text{m}^3$ ),  $\rho_0$  is the crude oil density ( $\text{kg}/\text{m}^3$ ),  $B_0$  is the crude oil formation volume factor ( $\text{m}^3/\text{m}^3$ ),  $E_o$  is the crude oil price (CNY/ $\text{m}^3$ ), and  $t$  is the waterflooding duration (days).

**Table 1.** Summary of oilfield water-treatment processes and associated costs

No.	Water-Quality Specification	Water-Treatment Process	Treatment Cost (CNY / $\text{m}^3$ )
1	xSuspended solids: 6mg/L; median particle diameter: $2\mu\text{m}$ ; oil content: 5mg/L	Installation of microfiltration units at pumping stations, backwash wastewater treatment during filter operation, bactericide dosing, aircyclone cleaning of trunk and branch lines, and well and line flushing	8.19(5.98 + 2.20)
2	Suspended solids: 0.45 mg/L; median particle diameter: $0.8\mu\text{m}$ ; oil content: 5mg/L	Installation of microfiltration units at pumping stations, backwash wastewater treatment during filter operation, bactericide dosing, aircyclone cleaning of trunk and branch lines, well and line flushing, and ceramic-membrane ultrafiltration	13.69(11.49 + 2.20)

The water-treatment method currently implemented in field operations is the dynamic-membrane treatment process. Its major cost components include the installation of microfiltration units at pumping stations, treatment of backwash wastewater during filter operation, bactericide dosing, air-cyclone cleaning of trunk lines (DN150) and branch lines (DN100), well flushing and line flushing, and ceramic-membrane ultrafiltration. For injection water

type 1-characterized by a suspended-solids concentration of 6 mg/L, a median particle diameter of 2  $\mu\text{m}$ , and an oil content of 5 mg/L-the total water-treatment cost is 8.19CNY/m<sup>3</sup>. For injection water type 2characterized by a suspended-solids concentration of 0.45 mg/L, a median particle diameter of 0.8  $\mu\text{m}$ , and an oil content of 5 mg/L-the treatment cost increases to 13.69 CNY/m<sup>3</sup>. Detailed watertreatment processes and cost components are presented in Table 1.

Taking the No. 8 Block reservoir as a representative example, the economic-benefit difference between these two injection-water qualities can be calculated using Eq. (3). The parameters adopted for this calculation are listed in Table 2, and the resulting economic benefits are shown in Figure 6 and Figure 7. The analysis indicates that the economic-benefit gap between the two water-quality grades widens progressively as injection time increases. Injection water with higher quality (suspended solids: 0.45 mg/L; median particle diameter: 0.8  $\mu\text{m}$ ; oil content: 5 mg/L) consistently yields a greater economic advantage relative to lower-quality water (suspended solids: 6 mg/L; median particle diameter: 2  $\mu\text{m}$ ; oil content: 5 mg/L). This trend is primarily attributed to the greater reservoir damage caused by larger particle diameters. With prolonged injection, the negative impact of inferior water quality on reservoir productivity becomes increasingly significant. Therefore, the injection-water quality should be improved under economically feasible conditions.

**Table 2.** Summary of waterflooding economic-benefit parameters

Parameter	Suspended Solids: 6mg/L; Median Particle Diameter: 2 $\mu\text{m}$ ; Oil Content: 5mg/L	Suspended Solids: 0.45mg/L; Median Particle Diameter: 0.8 $\mu\text{m}$ ; Oil Content: 5mg/L
$\alpha$ — formation-damage coefficient	1.0825	1.33
$\beta$ — formation-damage coefficient	-0.057	-0.07
$E_w$ — post-water-qualitydecision water-injection cost (CNY/m <sup>3</sup> )	5.98	11.49
$h$ — average reservoir thickness (m)		30.00
$K_0$ — reservoir permeability before waterflood adjustment (mD)		3.00
$p_e$ — supply pressure (MPa)		35.56
$p_{wf}$ — flowing bottom-hole pressure (MPa)		8.00
$r_e$ — equivalent drainage radius (m)		50.00
$r_w$ — wellbore radius (m)		0.07
$\rho_0$ — crude oil density (kg/m <sup>3</sup> )		0.68
$B_0$ — crude oil formation volume factor (m <sup>3</sup> /m <sup>3</sup> )		1.42
$f_w$ — water cut (%)		90.00
$E_0$ — crude oil price (CNY/m <sup>5</sup> )		79.50
$\phi$ — porosity		0.09
$\mu_o$ — crude oil viscosity (mPa · s)		2.84
$PV$ — pore volume (m <sup>3</sup> )		21205.71

Through the preceding analysis and economic evaluation, an injection-water quality standard that simultaneously ensures reservoir development performance and maintains economic viability can be effectively selected.

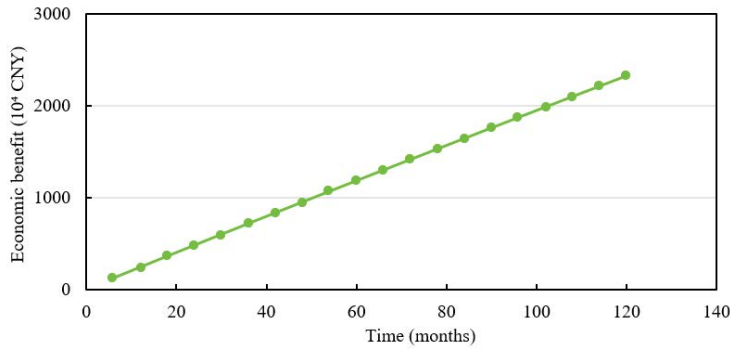


**Figure 6.** Economic benefit of injection water 1 (suspended solids: 6 mg/L; median particle diameter: 2  $\mu\text{m}$ ; oil content: 5 mg/L)

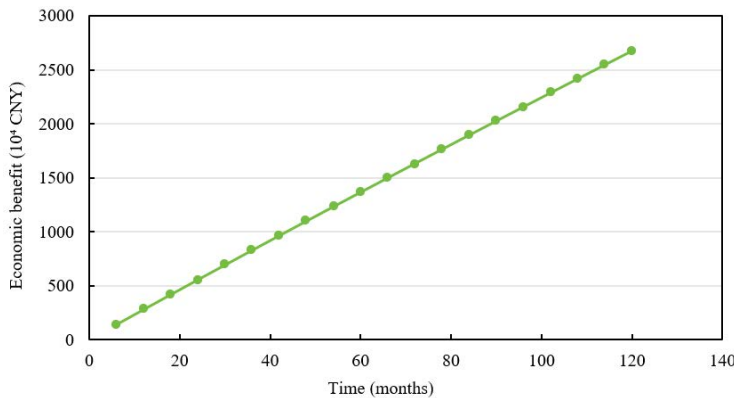


**Figure 7.** Economic benefit of injection water 2 (suspended solids: 0.8 mg/L; median particle diameter: 0.45  $\mu\text{m}$ ; oil content: 5 mg/L)

#### 4 Conclusions

A graded injection-water quality evaluation method and a corresponding apparatus designed for ultra-low-permeability fractured reservoirs were developed for the representative reservoir conditions in the No. 8 Block of the Xinjiang oilfield. Based on this method and apparatus, fracture–matrix core water-injection displacement experiments were conducted, leading to the following conclusions:

(a) In fracture-matrix cores with a matrix permeability of 8 mD, suspended particles with a median particle diameter  $\leq 1.5 \mu\text{m}$  and a concentration of 0.8–8 mg/L produced only minor permeability reduction. The permeability decreased from approximately 1.738 mD to 1.468–1.470 mD, corresponding to a permeability-impairment ratio of 15.48 %–17.32 %, all below the 20% compatibility threshold. The results indicate that suspended particles of this size range can be transported through the system without inducing significant formation damage. Particle retention occurred predominantly within the fracture segment, and the pressure drop increased most rapidly within the first 10 PV of injection.

(b) In systems with a fracture permeability of 20 mD, the fracture exhibited a pronounced capacity to intercept upstream particles. When the median particle diameter was 3  $\mu\text{m}$  at a concentration of 6 mg/L, the permeability decreased from 1.768 mD to 1.430 mD, resulting in an overall permeability-impairment ratio of 19.19% (< 20%), indicating acceptable transportability. When the particle concentration increased from 0.8 mg/L to 8 mg/L, the permeability-impairment ratio rose from 18.27% to 21.85%, and the most significant increase in pressure drop occurred during the early injection stage.

(c) An increase in particle size was found to substantially intensify permeability degradation. In the 8 mD system, enlarging the median particle diameter from 1.5  $\mu\text{m}$  to 3  $\mu\text{m}$  caused the permeability to decline to 0.532–0.677 mD, corresponding to permeability-impairment ratios of 37.75 %–52.42 %. These results indicate that maintaining both particle size and concentration within appropriate limits (median particle diameter  $\leq 1.5$ –3  $\mu\text{m}$  and concentration  $\leq 6$ –8 mg/L) is critical for ensuring that the permeability-impairment ratio remains below 20%.

(d) The economic assessment model constructed based on the permeability-decline characteristics under cumulative injection demonstrated that, although higher water-quality standards increased water-treatment costs from 8.19 CNY/m<sup>3</sup> to 13.69 CNY/m<sup>3</sup>, the improved water quality significantly slowed the long-term permeability

degradation and enhanced cumulative oil production, thereby yielding superior overall economic performance. This evaluation method and model provide a quantitative basis for selecting injection-water quality standards that simultaneously ensure reservoir protection and economic benefit in the fracture-matrix reservoirs of the No. 8 Block in the Xinjiang oilfield.

It should be noted that certain limitations remain in the present study regarding the experimental conditions and the number of repetitions. Several parameters were derived from a limited number of parallel experiments, and some degree of uncertainty persists. Future work will expand the experimental sample size and operating conditions to enable more systematic and refined validation and optimization of the permeability-decline mechanisms and the associated water-quality evaluation indicators.

## Data Availability

The data used to support the findings of this study are available from the corresponding author upon request.

## Conflicts of Interest

The authors declare that they have no conflicts of interest.

## References

- [1] X. Wang, H. Dang, and T. Gao, “Method of moderate water injection and its application in ultra-low permeability oil reservoirs of Yanchang Oilfield, NW China,” *Pet. Explor. Dev.*, vol. 45, no. 6, pp. 1094–1102, 2018. [https://doi.org/10.1016/s1876-3804\(18\)30112-5](https://doi.org/10.1016/s1876-3804(18)30112-5)
- [2] W. Hu, Y. Wei, and J. Bao, “Development of the theory and technology for low permeability reservoirs in China,” *Pet. Explor. Dev.*, vol. 45, no. 4, pp. 685–697, 2018. [https://doi.org/10.1016/s1876-3804\(18\)30072-7](https://doi.org/10.1016/s1876-3804(18)30072-7)
- [3] H. Kuang, G. Jin, and Z. Gao, “Sedimentary facies and evolution of the lower Urho Formation in the 8th area of Karamay oilfield of Xinjiang, NW China,” *Cogent Geosci.*, vol. 3, no. 1, p. 1333667, 2017. <https://doi.org/10.1080/23312041.2017.1333667>
- [4] L. Wang, H. Zhang, X. Peng, P. Wang, N. Zhao, S. Chu, X. Wang, and L. Kong, “Water-sensitive damage mechanism and the injection water source optimization of low permeability sandy conglomerate reservoirs,” *Pet. Explor. Dev.*, vol. 46, no. 6, pp. 1218–1230, 2019. [https://doi.org/10.1016/s1876-3804\(19\)60275-2](https://doi.org/10.1016/s1876-3804(19)60275-2)
- [5] J. Zhu, X. Tang, X. Li, Y. Wen, Z. Deng, D. Rao, Z. Yang, and C. Liu, “The reservoir injury rules of water injection to an ultralow permeability reservoir: Experimental research based on core-NMR and microfluidic technology,” *Energy Fuels*, vol. 38, no. 16, pp. 15 131–15 146, 2024. <https://doi.org/10.1021/acs.energyfuels.4c01797>
- [6] F. Razavirad, S. Heidari, and A. Shahrabadi, “Evaluation of compatibility between formation and Injection water into the Reservoir Rock,” *Colloids Surf. A*, vol. 690, p. 133787, 2024. <https://doi.org/10.1016/j.colsurfa.2024.133787>
- [7] Z. Liu, B. Shi, T. Ge, F. Sui, Y. Wang, P. Zhang, X. Chang, Y. Liu, Y. Wang, and Z. Wang, “Tight sandstone reservoir sensitivity and damage mechanism analysis: A case study from Ordos Basin, China and implications for reservoir damage prevention,” *Energy Geosci.*, vol. 3, no. 4, pp. 394–416, 2022. <https://doi.org/10.1016/j.engeos.2021.05.001>
- [8] D. Sun, “Microscale study on dynamics of particles in slurry filtrated through porous media,” *Comp. Part. Mech.*, vol. 11, no. 2, pp. 745–755, 2023. <https://doi.org/10.1007/s40571-023-00650-6>
- [9] B. Khuzhayorov, B. Fayziev, G. Ibragimov, and N. Md Arifin, “A deep bed filtration model of two-component suspension in dual-zone porous medium,” *Appl. Sci.*, vol. 10, no. 8, p. 2793, 2020. <https://doi.org/10.3390/ap10082793>
- [10] H. He, X. Xiong, T. Wu, R. Hu, Y. Chen, and Z. Yang, “Pore-scale study of particle transport and clogging mechanisms in a porous micromodel,” *Sep. Purif. Technol.*, vol. 362, p. 131929, 2025. <https://doi.org/10.1016/j.seppur.2025.131929>
- [11] Z. Li, H. Yang, Z. Sun, D. Nicolas Espinoza, and T. Matthew Balhoff, “A probability-based pore network model of particle jamming in porous media,” *Transp. Porous Med.*, vol. 139, no. 2, pp. 419–445, 2021. <https://doi.org/10.1007/s11242-021-01673-4>
- [12] D. Sun, “Hydrodynamics and effect of velocity on particle filtration due to bridging in water-saturated porous media using CFD–DEM simulation,” *Environ. Sci. Pollut. Res.*, vol. 30, no. 44, pp. 100 124–100 136, 2023. <https://doi.org/10.1007/s11356-023-29398-5>
- [13] A. Elrahmani, I. Riyadh Al-Raoush, H. Abugazia, and T. Seers, “Pore-scale simulation of fine particles migration in porous media using coupled CFD-DEM,” *Powder Technol.*, vol. 398, p. 117130, 2022. <https://doi.org/10.1016/j.powtec.2022.117130>

- [14] J. Won, J. Lee, and E. Susan Burns, “Upscaling polydispersed particle transport in porous media using pore network model,” *Acta Geotech.*, vol. 16, no. 2, pp. 421–432, 2020. <https://doi.org/10.1007/s11440-020-01038-z>
- [15] L. Bennacer, N. D. Ahfir, A. Alem, and H. Wang, “Coupled effects of ionic strength, particle size, and flow velocity on transport and deposition of suspended particles in saturated porous media,” *Transp. Porous Med.*, vol. 118, no. 2, pp. 251–269, 2017. <https://doi.org/10.1007/s11242-017-0856-6>
- [16] I. Bouhid de Aguiar, M. Meireles, A. Bouchoux, and K. Schröen, “Microfluidic model systems used to emulate processes occurring during soft particle filtration,” *Sci. Rep.*, vol. 9, no. 1, 2019. <https://doi.org/10.1038/s41598-019-39820-z>
- [17] G. Hu and D. Li, “Multiscale phenomena in microfluidics and nanofluidics,” *Chem. Eng. Sci.*, vol. 62, no. 13, pp. 3443–3454, 2007. <https://doi.org/10.1016/j.ces.2006.11.058>
- [18] L. Tang and Z. Zheng, “Tracking of re-injection of purified water in the second oil production plant of Karamay oilfield,” *J. Chengde Petrol. Coll.*, vol. 12, no. 2, pp. 30–33, 2010. <https://doi.org/10.13377/j.cnki.jcpc.2010.02.024>
- [19] X. Zhou, H. Zhang, Y. Long, M. Song, R. Qiu, Y. Yan, X. Yang, and Y. Liang, “Sustainable and clean oilfield development: Optimal operation of wastewater treatment and recycling system,” *J. Clean. Prod.*, vol. 252, p. 119819, 2020. <https://doi.org/10.1016/j.jclepro.2019.119819>
- [20] X. Zhang, D. Wei, and Y. Du, “Evaluation indexes and system for the quality stability of reclaimed water,” *Environ. Sci.*, vol. 43, no. 3, pp. 586–596, 2022. <https://doi.org/10.13227/j.hjx.202105276>
- [21] C. Senan, A. Surabhi, and M. Azhar, “Effect of temperature and calcium ion concentration on gelation and rheological properties of low methylated pectin,” *Asian J. Chem.*, vol. 30, no. 7, pp. 1671–1674, 2018. <https://doi.org/10.14233/ajchem.2018.21321>
- [22] T. Li, Y. Song, N. Wang, and X. Wang, “Research progress on the mechanism of dynamic membrane fouling during the softening process of nanofiltration membrane in brine solution,” *Chin. J. Appl. Chem.*, vol. 34, no. 4, pp. 367–378, 2017. <https://doi.org/10.11944/j.issn.1000-0518.2017.04.160351>
- [23] D. Ma, L. Ke, J. Zhang, and Y. Pan, “Evaluation methods and prospects of produced water compatibility and scaling tendency,” *Appl. Chem. Ind.*, vol. 49, no. 9, pp. 234–239, 2020. <https://doi.org/10.16581/j.cnki.issn1671-3206.20191104.016>
- [24] Y. Zhang, Z. Liu, X. Chen, W. Zhong, and Y. Ma, “Research status of influencing factors in the compatibility evaluation experiment of oil - and - gas - field produced water,” *Technol. Superv. Petrol. Ind.*, vol. 38, no. 8, pp. 13–18, 2022. <https://doi.org/10.20029/j.issn.1004-1346.2022.06.004>
- [25] L. Shi, “Research on the compatibility of injection water quality in block 4 - 1 and block 5 - 1 of karamay oilfield,” Ph.D. dissertation, China University of Petroleum (East China), Qingdao, 2019. <https://doi.org/10.27644/d.cnki.gsydu.2019.002158>